RoDSE Synthesized Fine Tailored Au Nanoparticles from $Au(X)_4^-$ (X = Cl^-, Br^-, and OH^-) on Unsupported Vulcan XC-72R for Ethanol Oxidation Reaction in Alkaline Media

Luis E. Betancourt, Ángel M. Ortiz-Rodríguez, Juan Corchado-García, and Carlos R. Cabrera*

Department of Chemistry, P.O. Box 70377, University of Puerto Rico, Río Piedras Campus, San Juan, PR 00936-8377

Abstract

An electrosynthesis method to obtain Au nanoparticles dispersed on carbon Vulcan XC-72R support material was done using AuX_4^- (X = Cl^-, Br^-, and OH^-) as molecular precursors and different electrolyte media. The Au surface structure was significantly enhanced using KOH as an electrolyte as opposed to KBr and H_2SO_4. Cyclic voltammetry was used as a surface sensitive technique to illustrate the Au/Vulcan XC-72R catalytic activity for the ethanol oxidation reaction (EOR). The Au electroactive surface area obtained were 1.88, 5.83, and 13.96 $m^2\ g^{-1}$ for Au/C-H_2SO_4, Au/C-KBr, and Au/C-KOH, respectively. The later compares to chemically reduced Au/C-Spheres that had an electroactive surface area of 15.0 $m^2\ g^{-1}$. The electrochemical Au electrodeposition, in alkaline media (Au/C-KOH), exhibited the highest catalytic activity for the EOR with a 50% increase in peak current density when compared with Au nanoparticles prepared by the chemical reduction route. Raman and X-ray photoelectron spectroscopies analyses of the Au/Vulcan XC-72R nanomaterials revealed a restructuring of the carbon functionalities responsible for the metal nanoparticle anchoring. Our results strongly suggest that the enhanced EOR catalytic activity is related to the presence of oxygen functional groups on the carbon surface, particularly ketonic groups on the carbon Vulcan XC-72R substrate.

Keywords: Gold, Vulcan XC-72R, RoDSE, Ethanol Oxidation Reaction, Electrodeposition

*To whom correspondence should be addressed: carlos.cabrera2@upr.edu

Introduction

Electrosynthetic methods have drawn great interest from researchers in academia and industry as the catalytic performance of metal nanoparticles continues to improve significantly over the past decade.[1] Current synthetic methods are strongly focused on the design of new properties using carbon supports while regulating size, morphology and crystallographic orientation, a staple for industrial applications.[2, 3] As such, typical synthetic methods have varied from seeded growth, chemical reduction, underpotential deposition and electrochemical methods, among others.[4] The deposition of metal nanoparticles onto carbon supports has substantially decreased the amount of noble metal loadings while also maintaining high activity. Many researchers have systematically investigated ways to synthesize larger scale amount of catalyst while maintaining high reactivity and high throughput that offer precise control of the active material.[5]

Among all the metal nanoparticles, gold nanoparticles (AuNPs) are the most stable with very important materials property.[6, 7] However, the size and dispersion of AuNPs are key for their application and further use. High surface area gold nanoparticles dispersed on carbonaceous substrates offer better electrocatalytic responses than their bulk counterparts. The structure and proper dispersal of the nanoparticles contribute to lower catalyst loading for fuel cell applications and higher surface area due to the substrate's high porosity.[8] Catalyst's support is essential for the proper dispersal of metal nanoparticles by acting as a path of electron transfer, increasing electrical conductivity while reducing precious metal loading. Vulcan XC-72R is the most common commercial carbon black support consisting of quasi-spherical carbon particles with < 50 nm in diameter and with polycrystalline structures of several layers with an interplanar separation of 0.55-0.38 nm and a surface area of ca. 250 m^2 g^{-1}.[9] It has been reported that the behavior of the carbon black as a catalyst support is dependent on its specific characteristic, as

well as on different treatments used.[10] Although several studies have focused on the effect of the support functionalization on the physico-chemical properties of Pt catalysts. However, there is still need to address the effect of functionalization in alkaline media for Au nanoparticles.

Recently, an electrochemical method known as Rotating Disk Slurry Electrode (RoDSE) technique has been developed to prepare highly dispersed bulk carbon-supported metal nanoparticle catalysts with high surface area.[11] The RoDSE technique has been used to electrochemically prepare bulk Au/carbon nanocatalyst material. This was done by using a slurry solution saturated with functionalized Vulcan XC-72R to which a gold precursor was added and an electrochemical rotating disk electrode route was used to prepare the Au/carbon catalyst bulk sample. Herein, we present an electrosynthetic method able to deposit Au nanoparticles without the need of a protective or stabilizing agent with controlled size, shape and dispersion resulting in the ideal mass production method of Au electrocatalysts. In addition, with the RoDSE technique, instead of growing films over large areas, it is possible to electrodeposit nanoparticles on a highly dispersed substrate like Vulcan XC-72R,[11] carbon nanoonions,[12] single-wall carbon nanotubes,[13] and electrochemically reduced graphene oxide[14]. The working electrode area limits strategies using electrodeposition techniques such as using RDE electrodes to deposit platinum nanoparticles on a Nafion modified carbon electrode. Therefore, the technique is limited to the size of the electrode working area and is unable to mass produce the amount of catalyst needed for a fuel cell system.[15] On the other hand, nanocatalysts prepared by the RoDSE technique produces bulk quantities of carbon supported nanocatalysts while also avoiding agglomerations of the nanoparticles.

In this paper, the intrinsic importance of the electrolyte media and its carbon support effect in the RoDSE technique is being presented. The RoDSE parameters are critical factors that determine

the Au nanoparticle size, morphology, and performance for the ethanol oxidation reaction (EOR). To this end, the RoDSE technique was used to electrochemically deposit Au NP onto unsupported Vulcan Carbon XC-72R at different electrolyte slurry solutions. The Au RoDSE deposition catalyst was studied in H_2SO_4, KBr and KOH under the formation of $Au(X)_4^-$ (X = Cl^-, Br^-, and OH^-) molecular precursors.[16, 17] In these electrolytes, $Au(Cl)_4^-$ will be in the form of Au(III) halide and hydroxide complexes. The chemical-physical properties, related to the catalytic EOR behavior, were determined for the RoDSE catalyst prepared with these electrolytes and $Au(X)_4^-$ molecular precursors. Our findings revealed that interaction between the carbon support and the electrolytic media used for the Au electrodeposition influences greatly the nucleation sites created during the synthesis and the EOR properties.

Methodology

Materials

Tetrachloroauric acid trihydrate [$HAuCl_4*3H_2O$] (ACS grade, Aldrich), sulfuric acid (H_2SO_4) (Optima, Aldrich), potassium bromide (KBr) (ACS grade, Aldrich) and potassium hydroxide (KOH) (ACS grade, Aldrich) were used as received. All the solutions were prepared using ultra-pure water (Milli-Q, Millipore, 18.2 MΩ-cm).

Instruments and methods

Electrochemical experiments were done at room temperature (T = 294 K) in a three-electrode cell separated by a porous membrane between each chamber. The electrochemical measurements were done using a 600E Potentiostat/Galvanostat Electrochemical Workstation (CH Instruments, Inc.). A commercial rotating disk glassy carbon (GC) electrode (PINE Research Instrumentation, Inc.) was used as the working electrode, a reversible hydrogen electrode (RHE) and a platinum wire were used as a reference and counter electrodes, respectively. Therefore, all potentials are referenced against the RHE reference electrode. Before the AuNPs deposition on carbon Vulcan

substrate (Vulcan XC-72R; Cabot Corporation), the rotating disk GC electrode was polished to a mirror-like finish using alumina with different powder sizes (i.e. 1 μm, 0.3 μm, and 0.1 μm alumina) and thoroughly washed with 18.2 Ω-cm dionized water.

RoDSE Method

The RoDSE method consists on dissolving a metal precursor, in this case $HAuCl_4 \cdot 3H_2O$, in a colloidal carbon support slurry solution as has been reported elsewhere by our group.[11, 18] Here, different electrolytes were used in the Au electrodeposition process, i.e. H_2SO_4, KBr, and KOH. In KOH and KBr, $AuCl_4^-$ will be in the form of $Au(OH)_4^-$ and $Au(Br)_4^-$, respectively.[16] Briefly, 50.0 mg of Vulcan XC-72R were weighed and dissolved in 20.0 mL of 0.10 M H_2SO_4, 0.10 M KOH or 0.01 M KBr and maintained under ultrasound conditions for 1 hour. The slurry suspension was then transferred to the working electrode compartment in a three-electrode cell separated by glassed frits (0.20 cm^2 geometric area). Afterwards, 2.00 mL of a 5 mM $HAuCl_4$ metal precursor was added under vigorous stirring to the working electrode compartment. A rotor (PINE Research Instrumentation) was used to adjust the rotating disk glassy carbon electrode rotating speed to 2,000 rpm in the slurry solution. Gold electrodeposition was done using a chronoamperometry setup with an applied potential of 0.700 V vs. RHE for each of the electrolytes used (0.10 M H_2SO_4, 0.10 M KBr and 0.10 M KOH). The chronoamperometry process was repeated three additional times with the addition of 2.00 mL of 5 mM $HAuCl_4$ aqueous solution in each repetition. Finally, the product catalyst slurry solution was filtered and rinsed with 500 mL of ethanol and 500 mL of water previously distilled and deionized to 18.2 MΩ-cm conductivity. The resulting filtered catalyst nanomaterial was heated on a conventional oven to 100 °C and grinded to a fine powder to further characterize its physical, chemical, and electrochemical properties.

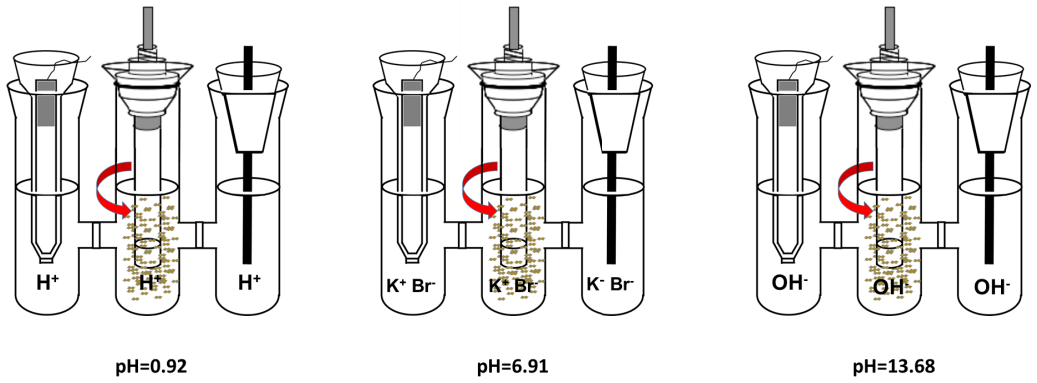

Figure 1. Schematic of the Au/Vulcan XC-72R nanoparticle synthesis setup in each electrolyte media with its corresponding pH, 0.92 for H_2SO_4, 6.91 for KBr, and 13.68 for KOH. The 3-compartment electrode cell diagram corresponds from left to right to a reversible hydrogen electrode reference electrode, glassy carbon rotating disk working electrode and Pt auxiliary electrodes.

Reduction synthesis

In order to compare our electrochemically synthesized catalyst with the chemical reduction route, quasi-spherical carbon supported Au NPs were prepared in a process described elsewhere by Sánchez-Sánchez et al.[19] Briefly, it consisted on preparing an ice-cold solution of 0.01 M $NaBH_4$ where 0.3 mL was mixed with 8 mL of 5mM Au^{3+} solution along with 10 mL of trisodium citrate dehydrate (2.5×10^{-4} M) with vigorous stirring under room temperature. After 30 s stirring, the Au colloid solution was stirred vigorously at 45 ^{0}C for 15 min to ensure reaction of the excess reducing agent. Then, 50 mg of carbon Vulcan XC-72R powder was added under fast stirring for approximately 1 h. Finally, NaOH pellets were added to the mixture to precipitate the sample and the synthesis was left overnight.

GCE modification

Glassy carbon (GC) electrodes (3 mm diameter, from BASi) were used to test the Au catalysts prepared by RoDSE and chemical methods. Before using the electrode for the catalyst electrochemical characterization, the GC electrode was mechanically and electrochemically

cleaned. The first step was to polish the electrode until a mirror-like finish was obtained using Alumina powder. Then, the GC electrode was subjected to 5 potential cycles from 0.0V to 1.2 V vs. RHE at 100 mV/s in 0.1M KOH to ensure that the surface was within surface cleaned working conditions. Later, a slurry solution was prepared with the synthesized catalyst in which 1.00mg of AuNP/Vulcan catalyst was weighed and dissolved in 440μL of ethanol and 10 μL of Fumion FAA-3 ionomer solution (10 wt% in N-methyl-2-pyrrolidone (NMP), FuMA-Tech Inc.). Ultrasonication was followed to disperse the slurry solution and make an ink. After the ink preparation, 8μL of the ink was drop casted on the surface of a previously polished GC Electrode and was left to dry in air. Electrochemical measurements consisted on cyclic voltammetry (CV), linear sweep voltammetry (LSV), and chronoamperometry. A 3-electrode system was used for the electrochemical measurements. The working electrode consisted on the Au catalyst modified GC electrode, a Pt mesh as an auxiliary electrode and a Reference Hydrogen Electrode (RHE).

Spectroscopic Characterization

X-ray diffraction patterns were collected with a RIGAKU SmartLab diffractometer in reflectance Bragg-Brentano geometry using Cu K_α radiation (λ=1.5406 Å), with a tube current of 44 mA and a tube voltage and 40 kV power, equipped with high-speed 1D detector (D/teX Ultra).

The Au/C catalyst were characterized using a transmission electron microscope (FEI Tecnai F20) with an operation voltage of 240 kV equipped with a monochromator and an Oxford SDD X-ray detector.

X-ray photoelectron spectroscopy (XPS) (PHI 5600ci) was performed with a Mg Kα monochromatic X-ray source (350 W) and a hemispherical electron energy analyzer. For XPS, a small amount of the catalytic powder was pressed onto a Carbon tape. The XPS results for the Au 4f binding energy region was analyzed using a curve-fitting program (Multipack) for peak

deconvolution. All the binding energies reported were corrected fixing the carbon peak (C 1s) at 284.5 eV. The peak assignments for the C 1s components are shown in Table 1.[20]

Table 1. Peak assignments for the C 1s components

Carbon 1s Components	**Binding Energy (eV)**
Graphite (sp^2)	284.4
C-H (sp^3)	285.0
C-OH / C-O-C (sp^3)	286.1 – 286.3
C=O	287.6 – 287.7
COOH / COOR	288.6 – 289.1
π-π*	290.5 – 290.8

The peak assignment for the Au 4f binding energy peak components were: 83.8 and 87.5 eV for Au^0 $4f_{7/2}$ and $4f_{5/2}$[21] and 85.9 and 89.6 eV for $Au_2O_3/Au(OH)_3$[21]. The $[AuBr_4^-]$ $4f_{7/2}$ and $4f_{5/2}$ peaks were approximated from the $CsAuBr_4$ peaks at 87.0 and 90.6 eV[22], respectively.

The Au catalyst loading was determined by thermogravimetric analysis (TGA) and further confirmed by inductively coupled plasma-atomic emission spectroscopy (ICP-AES, Perkin Elmer 4300l DV). TGA was done in air with a temperature ramp of 10 °C min^{-1} using a Perkin Elmer STA 6000.

Raman Spectra

Raman scattering experiments were done using a Jobin Yvon Horiba LabRam HR 800 Raman microscope with a laser source with a wavelength of 632nm. Constant unfiltered laser beam irradiation was maintained for some minutes prior to the data collection in order to reach the necessary equilibrium and to minimize the temperature variation of the sample during the measurements. To point out and map the most interesting zones of the samples an X–Y stage for spectral mapping was used. The measurement error was ±2 cm^{-1}. All the Raman spectra were analyzed by fitting the spectra with different numbers (from one to five) of Lorentzian line

shapes, using the Fityk mathematical package. The criterion of best fit was taken as the maximum value of the determination coefficient (R^2).

Results and Discussion

Voltammetric Analysis of RoDSE Electrodeposition

To assess the optimal electrodeposition potential, a cyclic voltammetry was done using a GCE working electrode in a solution of the metal precursor ($HAuCl_4$) in each of the electrodeposition (0.1M KOH, KBr and H_2SO_4) electrolytes. **Figure 2** shows the cyclic voltammogram of 5 mM $HAuCl_4$ in 0.1 M KOH at a glassy carbon electrode at a scan rate of 100 mV/s. At this KOH concentration, $AuCl_4^-$ will form $Au(OH)_4^-$.[23, 24] The behavior of the solution was assessed starting the potential from 1.6 V up to 0 V vs. RHE for a total of 5 scans. The voltammetries in 0.1 M H_2SO_4 and 0.1M KBr are shown in **Figure S1**. Close examination of the voltammetry profile in each electrolyte show distinctive reduction peaks. On the first cycle, a reduction peak was observed *ca.* 0.820 V vs. RHE during the forward scan. This reduction peak, in 0.1 M KOH, is only visible on the first scan and is attributed to the reduction of Au (III) to Au^0 on the bare GCE according to the following equation:[24]

$$Au(OH)_4^-(aq) + 3e^- \rightarrow Au^0(s) + 4OH^-(aq) \qquad \text{(Eq. 1)}$$

In the backward scan, an anodic peak is observed at 1.2 V vs. RHE obeying the following equation:

$$Au(s) + 4OH^-(aq) \rightarrow [Au(OH)_4^-](aq) + 3\ e^- \qquad \text{(Eq. 2)}$$

From the second cycle onward, a film of gold deposited on the GCE during the forward scan is already present since the first cycle, therefore the subsequent Au deposition occurs on the gold active site formed at the electrode surface. Note that the first cycle's forward scan reduction peak is no longer visible and from the second scan onwards, two distinctive reduction peaks are

observed at 1.2 and 1.1 V vs. RHE. The small reduction peak at 1.2 V corresponds to the $[Au(OH)_4]^-$ to $[Au(OH)_2]^-$ reduction. These complexes are not stable in solution and dissociate further into Au^0 and $[Au(OH)_4]^-$. The 1.2 V peak is attributed to the reduction of Au (III) to Au^0 on the trace amount of gold remaining on the GCE after the first cycle. **Figure 2** shows a fingerprint of the electronic behavior of $HAuCl_4$ in alkaline electrolyte while the voltammetries in the other electrolytes are shown in the ESI. Slight differences between reduction potentials in each electrolyte are most likely due to differences in the adsorption strength of the anions in solution and the formation of $Au(OH)_4^-$ in alkaline media.[25] It is well documented that there are no competitive anions in the alkaline electrolyte as opposed to an acidic or neutral environment. The electrodeposition done in neutral media (KBr) showed an interesting behavior where the stable $AuBr_4^-$ is formed according to an EC mechanism.[26] Furthermore, 0.7V vs. RHE is close to the Au (III) to Au^0 redox potential in each electrolyte, and s was used as the electrodeposition potential for the RoDSE synthesis.

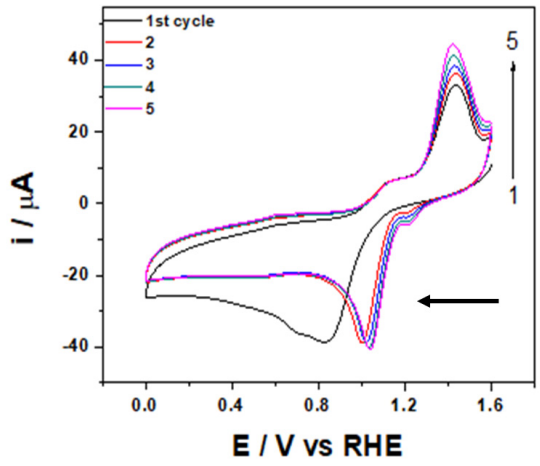

Figure 2. Cyclic voltammetry profile of Au electrodeposition in 5mM in $HAuCl_4$ in 0.1M KOH alkaline media using a Glassy Carbon Electrode and a scan rate of 20mV/s at room temperature. The arrow shows the first potential cycle direction starting at 1.6 V vs. RHE.

Gold electrodeposition using the RoDSE Method

The electrodeposition using the RoDSE method gave a distinct voltammetry profile shown in **Figure 3**. The typical current-time curve corresponds to an instantaneous nucleation and diffusion-limited growth.[27] The key parameters in this modality for chronoamperometry were the applied potential and potential time duration. **Figure 3** shows the chronoamperogram of 5mM $HAuCl_4$ in 0.1M KOH with Vulcan XC-72R on the rotating GC electrode for 4 consecutive 2.00 mL aliquot additions every 2 hours. A small hump at 100s was observed in the cathodic transient corresponding to an induction period of nucleation on the GC electrode. The cathodic current increase can be explained by the nucleation of gold on the GC electrode as well as an increase in the rate of mass transfer around the particle. Then, the current decreased following transient decrease as the amount of $HAuCl_4$ present in solution decreased.

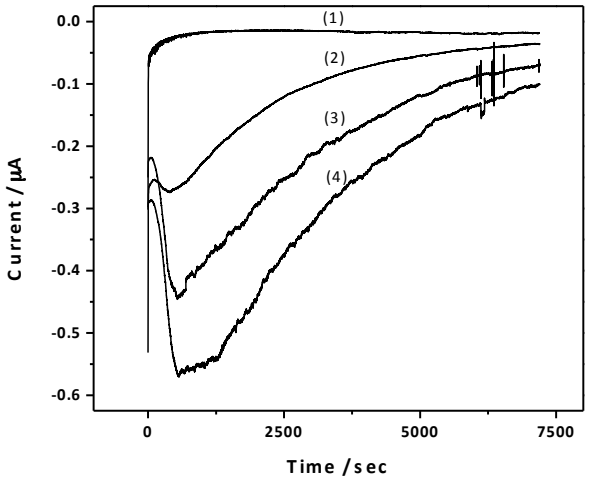

Figure 3. Au electrodeposition chronoamperometry profiles for AuNPs/C in 50.0 mg of Vulcan XC-72R in 20.0 mL of 0.100 M KOH using a GC RDE at a rotating speed of 2,000 rpm and an applied potential of 0.700 V vs. RHE. The chronoamperometric process was repeated three additional times with the addition of 2.00 mL of 5 mM $HAuCl_4$ in each repetition.

Au electrodeposition occurs at the carbonaceous substrate due to rotations of the RDE attracting the Vulcan XC-72R towards the disk due to the hydrodynamic effect of the rotation. When the carbon support is near the GC rotating disk electrode, Au is electrodeposited. We believe that the process involves the reduction of Au^{3+} salt when the ions are in close contact with the GC electrode and the unsupported carbon substrate, and when it becomes charged by coming in close contact to the GC rotating disk electrode where Au ions can be reduced. It is interesting to note that since Vulcan XC-72R is a complex matrix with diverse functionalities, we expect to obtain different oxygen moieties as a function of pH and their modification at the applied potential. Note that to carry out this electrodeposition, it is necessary for the slurry to become homogenized and the hydrodynamic effect due to the RDE rotations helps with the dispersion of the carbon support.

Transmission Electron Microscopy

Transmission electron microscopy (TEM) was used to determine the Au nanoparticle size, shape, and dispersion within the Vulcan XC-72R carbon support**. Figure 4** shows TEM images of Au NPs deposited on carbon using different electrolytes for Au electrodeposition. These images show that Au NPs are synthesized in different shape and sizes depending on the respective chemical environment used for their electrodeposition. The Au nanoparticles were presented as dark spots on a lighter background of the carbon support. Remarkable differences were found, as expected, from the different synthetic methodologies used. **Figure 4 (a-c)** shows the resulting powder after electrodeposition in H_2SO_4 where minimal dispersion can be observed and the size of the particles were approximately 50 nm with no preferred facet or defined morphology. Meanwhile, using KBr as an electrolyte, the nanoparticle size went down to 30-40 nm. However,

a low dispersion of AuNPs was observed. On the other hand, HR-TEM images of the Au nanoparticles deposited in alkaline media exhibit an average nanoparticle size of 7 nm with significantly higher dispersion. The sphered nanoparticles deposited using the reducing agent treatment are shown in Figure S2. [19]

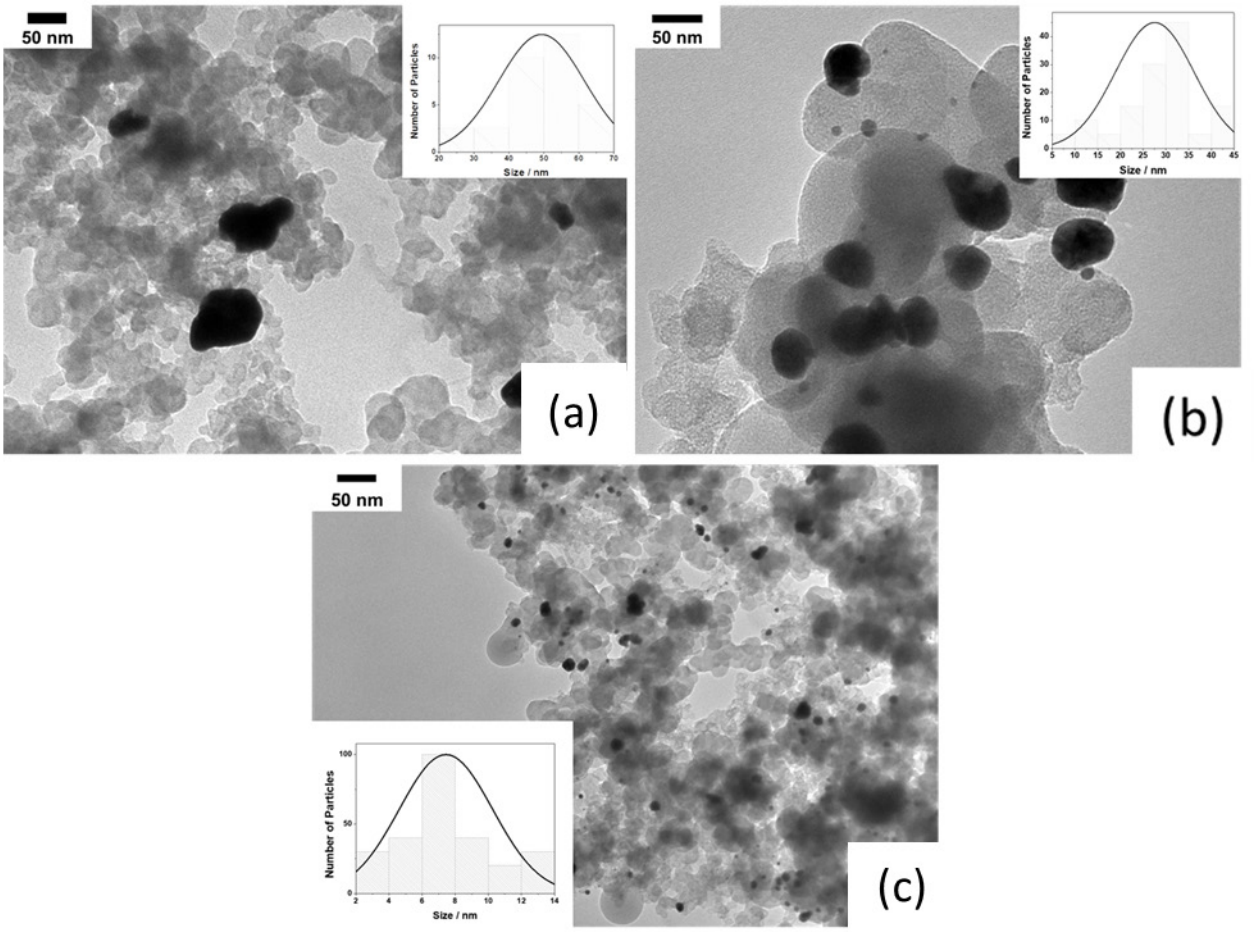

Figure 4. Transmission electron microscopy images of carbon supported Au nanoparticles electrodeposited by the RoDSE technique: (a) Au/C-H_2SO_4 (b) Au/C-KBr (c) Au/C- KOH.

X-ray Diffraction

The TEM data gave information regarding the nanoparticles size, shape, and dispersion, but nothing about their surface structure, which is also relevant to reactivity. Surface structure is well

associated to reactivity at gold electrodes for alcohol oxidation.[28] TEM data shows valuable information regarding nanoparticle size and morphology, as well as how disperse they are on the carbon substrate, but nothing regarding their surface and crystal structure. For that matter, X-ray diffraction was done on all of the Au/C samples. Catalysts showed typical fcc Au diffraction pattern with peaks located at 2θ equal to 38°, 44°, 64° corresponding to the (111), (200) and (220) facets, respectively. Au/C-Spheres obtained via chemical reduction route were used in this study to compare its activity and structure to the RoDSE deposited catalysts.

However, it is well known that nanoparticle shape is characteristic for its surface structure. The electrochemical activity of a molecule is closely related to the facility of the surface electrons of the particles to promote a catalytic process. Therefore, different reactivity can be expected to be obtained on different reflectance planes of a fcc metal such as gold.[28] Au/C electrodeposited on alkaline media have a preferential (111) plane as compared to the other sample's surface orientation. Consequently, electrocatalytic activity is expected to vary across these samples as a result of different surface structure. The intensity ratio between the (200) and (111) diffraction, $I_{(200)}/I_{(111)}$, were calculated and revealed different values than the conventional bulk intensity ratio (≈0.53).[29] The $I_{(200)}/I_{(111)}$ peak intensity ratios calculated were 0.33, 0.33, 0.27 and 0.27 for samples Au/C-H_2SO_4, Au/C-KBr, Au/C-KOH and Au/C-Spheres, respectively. On the other hand, the full width half maximum (FWHM) of the XRD peaks was used to evaluate the size differences of the samples. The average Au crystal size was calculated based on the Au (111) diffraction peak using the Debye-Sherrer formula shown below:

$$L = \frac{0.9\,\lambda_{K\alpha}}{B_{2\theta}\cos\theta_{max}}$$

Where L is the mean crystallite size, λ is the wavelength of the x-rays (1.5406 Å), B is the full width-half-maximum of the peak and θ is the Bragg angle of the Au (111) peak. The average crystallized sizes obtained were 65 nm, 45, 10 nm for H_2SO_4, KBr and KOH, respectively, which is consistent with the TEM nanoparticle sizes.

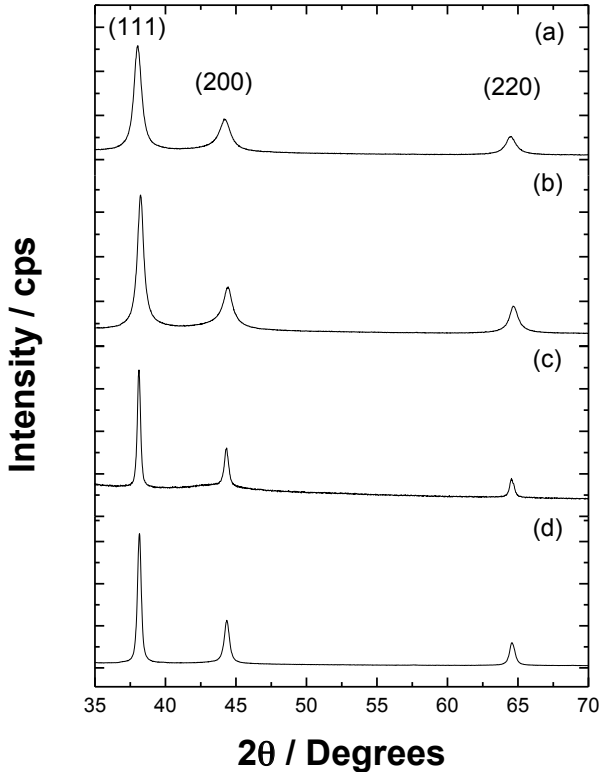

Figure 5. X-ray diffraction pattern of Au/C deposited in a) KOH, b) KBr, and c) H_2SO_4 - electrolytes and (d) by chemical reduction.

Thermogravimetric Analysis

TGA analyses were done on four carbon-based catalysts, previously described, to determine the metal loading. Before analyzing the supported materials, TGA (see **Figure 6**) measurements of carbon Vulcan-XC72 were performed to further explore their influence in the presence of the metal nanoparticles reaction occurring. **Figure 6** shows the TGA of Au/C samples for Au/C-

H_2SO_4, Au/C-KBr, Au/C-KOH and Au/C-Spheres, with Au percent loadings of 16%, 6%, 10% and 11%, respectively. Subsequently, the labile oxygen functional groups will evaporate to carbon oxide gas species, which is followed by the oxidation of the carbon left by the high temperature in air. Vulcan XC-72R TGA ended at 0% after reaching 1000 °C.

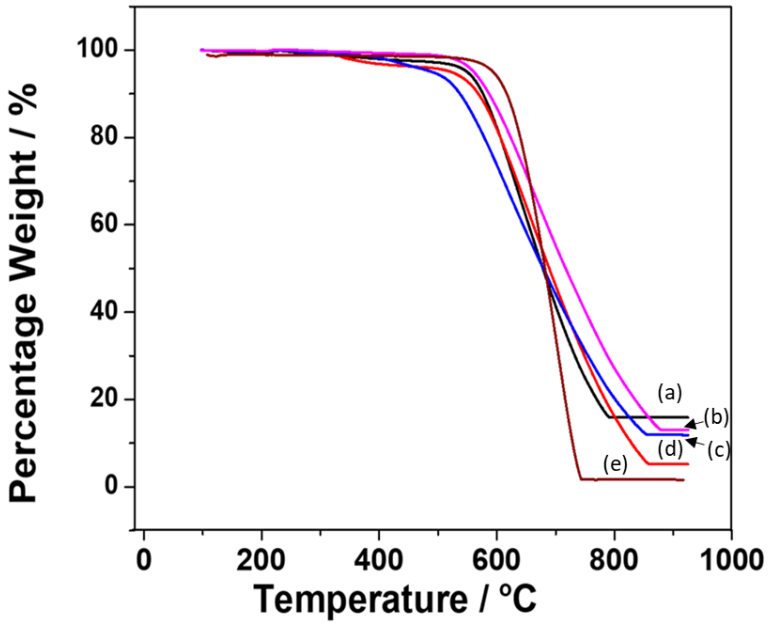

Figure 6. Thermogravimetric analysis data curves at 100 mL^{-1} airflow and 5°C-min^{-1} linear temperature ramp variation of the support and with nanoparticles. (a) Au/C-H_2SO_4 (black), (b) Au/C-KBr (red), (c) Au/C-KOH (blue), (d) Au/C-Spheres (magenta), and (e) Vulcan XC-72R (burgundy).

X-ray Photoelectron Spectroscopy Analysis

To understand the effect of the synthesis medium on the gold nanoparticles electrodeposition on Vulcan XC – 72R, X-ray photoelectron spectroscopy (XPS) analysis was performed for each catalyst. **Figure 7** shows the XPS C 1s and Au 4f spectra obtained for the synthesized samples,

as well as the peak deconvolution. The C 1s binding energy peak contains various features that could not be fully resolved. Instead of fitting all 6 components, the peak deconvolution was carried out as previously described in **Table 1** and the contribution for each component of the C 1s and Au 4f are described in **Table 2**.

Table 2. Deconvoluted contribution for the C 1s and Au 4f binding energy components of the XPS measurements for each synthesized Au catalyst.

	Carbon 1s Component % Contribution					Gold 4f Component % Contribution		
Sample	sp^2/ C-H	C-OH/ C-O-C	C=O	COOH / COOR	π-π*	Au^0	Au_2O_3/ $Au(OH)_3$	$KAuBr_4$
Au Spheres	68.4%	18.3%	4.8%	5.1%	3.4%	97%	4%	0
Au/C-H_2SO_4	60.9%	21.6%	8.6%	4.3%	4.6%	78%	23%	0
Au/C-KBr	71.5%	15.3%	5.4%	3.5%	4.3%	47%	13%	40%
Au/C-KOH	74.3%	12.2%	5.1%	2.9%	5.6%	94%	6%	0

To determine the surface oxidation state of the Au/C catalysts and carbon support, XPS was used. Since the Au particles are in the nanometer range, the surface oxidation state of the metallic nanoparticles will reflect the bulk oxidation state. Au 4f and C 1s binding energy region spectra for the electrodeposited materials are shown in **Figures 7** and **8**. The relative contributions of each C 1s component are summarized in **Table 2**.

The Au 4f binding energy signal consisted of two pair of doublets, $4f_{5/2}$ and $4f_{7/2}$. The most intense doublet is assigned to metallic Au. The second doublets were at ca. 1.8 eV higher binding energy than that for Au (0). This is attributed to the Au (III) chemical state, as in Au_2O_3 or $Au(OH)_3$. Comparing the Au 4f spectra of the various chemical-treated carbon-supported catalysts, it was observed that the Au-H_2SO_4 and Au-KBr samples, in comparison with Au-KOH

and Au-Spheres, had a higher content of oxidized Au (III) and a lower content of Au (0). In addition, the KBr sample showed two additional binding energy peaks corresponding to the stable complex $KAuBr_4$.

The C_{1s} binding energy spectrum appeared to be composed of graphitic carbon (284.7 eV) and -C=O- like species (285.8 eV). A small amount of surface functional groups with high oxygen contents was also noted in the spectrum (>287.6 eV). The Au-KOH exhibits the lowest oxygen contents with a 74.3% of graphitic C-H. Undoubtedly, the carbon chemical environment influenced in the Au uptake and further reactivity. The main component of the C 1s region for the carbon samples is the symmetric peak at ~284.2 eV, which corresponds to non-functionalized carbon support (present in sp^2 and sp^3 hybridized state in aromatic rings or in aliphatic chains). This relative peak percentage for this symmetric peak was the highest (except for KOH treatment), which indicated that most of the surface carbon atoms were present in a non-functionalized state. The increase in the binding energy peak at 285 eV, observed for the carbons treated other than KOH, would indicate the formation of C-O bonds. The set of peaks with binding energies around 285 eV can be attributed to the carbon bonded to oxygen pointing to the probable functionalities being hydroxyl or ether groups which were the main functionalities detected.

The surface oxygen groups decrease the hydrophobicity of the carbon, thus making its surface more accessible to the metal precursor during the impregnation in aqueous solution. Furthermore, these O_2 surface groups are credited with acting as nucleation sites. Hence, the Au-H_2SO_4 exhibited a higher oxidized carbon content and in addition a higher Au uptake in accordance to the TGA data. However, this uptake comes at a price since it led to agglomeration of the nanoparticles as was observed by TEM and confirmed by XRD analysis.

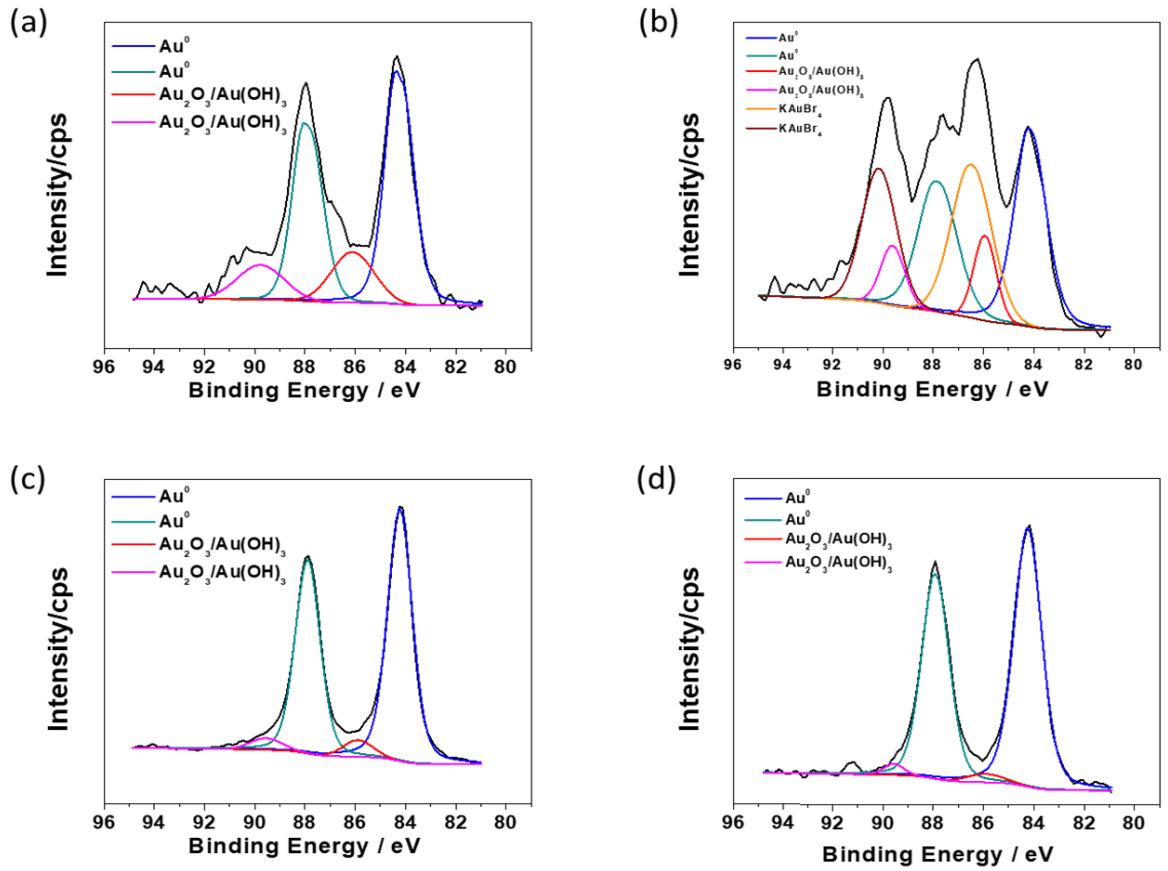

Figure 7. X-ray photoelectron spectroscopy deconvolution of the Au 4f binding energy region for Au/C nanoparticles deposited in (a) acidic (b) neutral (c) alkaline and (d) Au spheres reduced using $NaBH_4$ as a reduction agent.

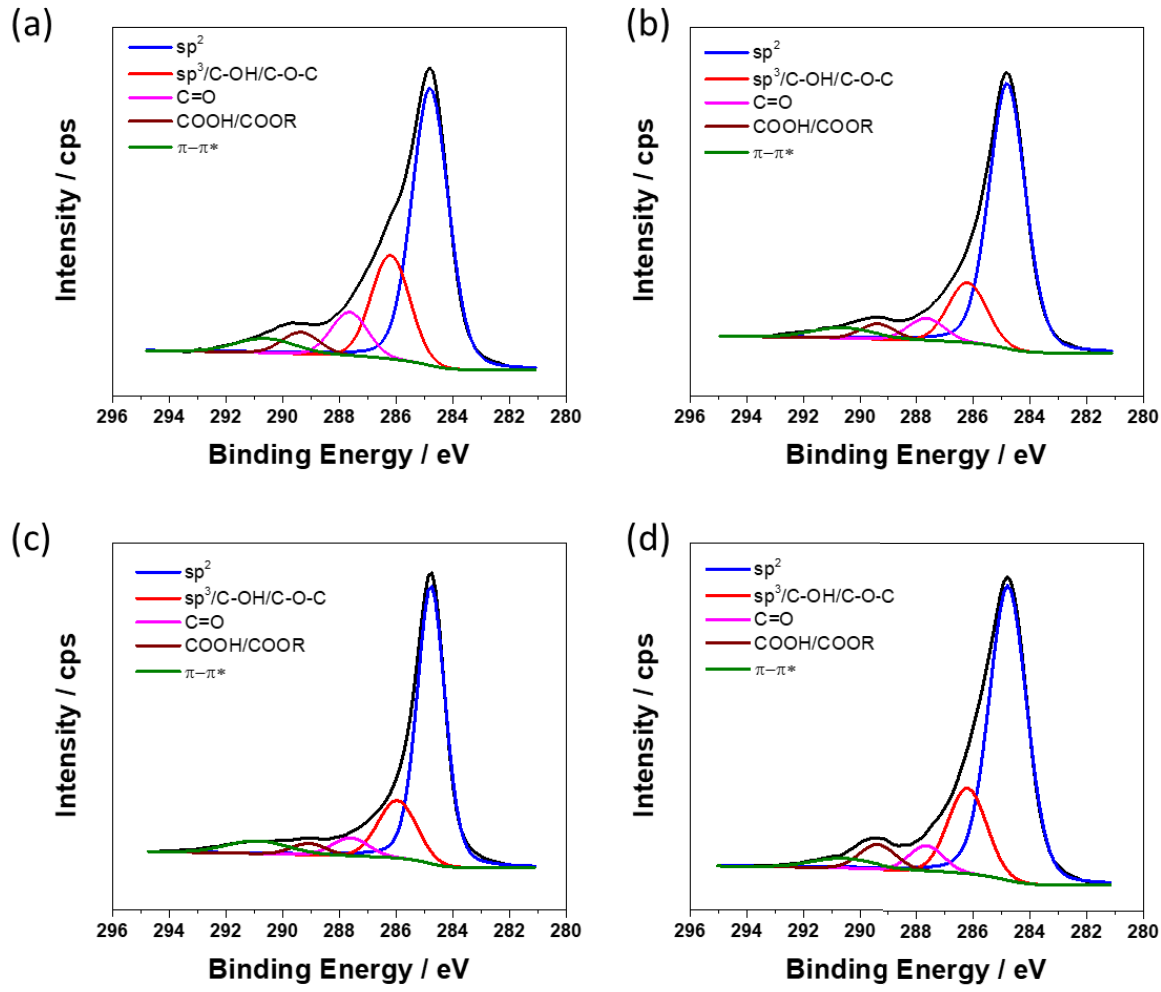

Figure 8. High resolution X-ray photoelectron spectroscopy deconvolution of Au/C nanoparticles deposited in (a) acidic (b) neutral (c) alkaline and (d) Au spheres reduced using $NaBH_4$ as a reduction agent. Peak deconvolution corresponds to the C 1s transition.

Raman Spectroscopy

Raman spectroscopy was used to gain insight into the nature of the carbon species on the carbon substrate. A curve fitting was carried out for each spectrum to determine spectroscopic parameters such as peak position, band intensity and line shape. The main contributing crystalline forms of carbon: graphitic and diamond have been well studied. The diamond has a face centered cubic crystallographic structure and is characteristic of the C-C single bonds between sp^3 hybridized carbon atoms with a band located at 1332 cm^{-1}. The G-band

corresponding to the E_{2g} symmetry is localized around 1602 cm^{-1}. The amorphous sp^2 phase of carbon appears ca. 120 cm^{-1} between the D and G bands while the sp^3 rich phase appears centered at 1180 cm^{-1}. The resulting Raman line decomposition is shown in **Figure 9** in accordance to recent work carried out on amorphous carbon. A decomposition of bands between 1200 and 1800 cm^{-1} was carried out. The curve fitting was carried out according to previous works were two Lorentzian lines around 1360 and 1600 cm^{-1} and a broad Gaussian band were used. It is well known that the behavior of activated carbon supported materials catalysts can be modified by oxidation treatment of the support prior to metal loading. The degree of graphitization of these carbonaceous materials (I_D/I_G ratio) is used to quantify the number of defects in the carbon-based materials. Figure S3 shows the carbon substrate modification in acidic and neutral media used for electrodeposition, which gave a similar D/G ratio as Vulcan XC-72R suggesting no restructuring of surface sites. On the other hand, in alkaline media, the substrate showed a decrease in ratio, in effect showing a higher area for the graphitic peak and sp^2 rich phase as confirmed by the XPS analysis. The higher I_D/I_G can be attributed to the extensive graphitic destruction induced by the harsh oxidative environment used for the production of Vulcan XC-72R. However, a restructuring of the surface sites in alkaline media seem responsible for the observed differences in the Raman spectra.

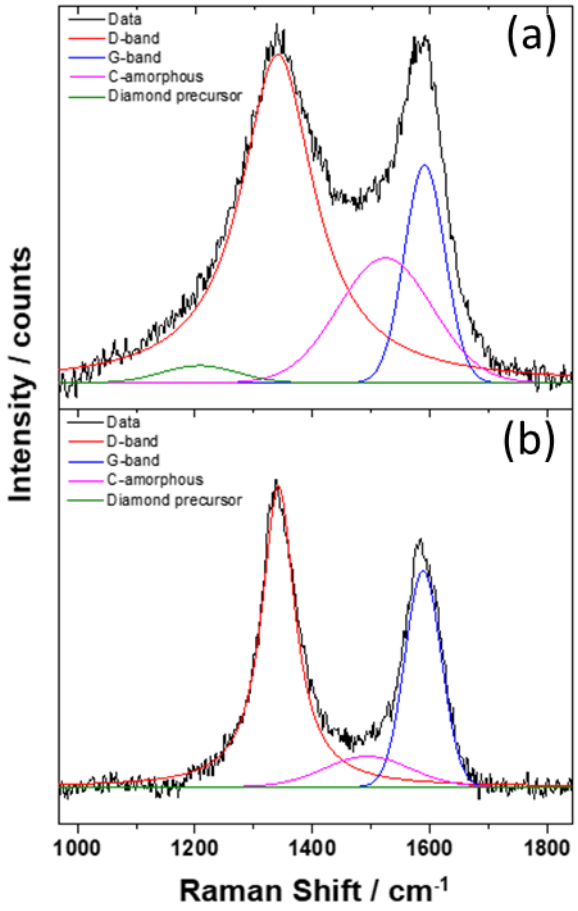

Figure 9. Raman spectra of the pretreated (a) Vulcan XC 72R and treated (b) Au/C-KOH catalyst.

Electroactive Surface Area (EASA) Determination

While the physical characterization tools determined the average nanoparticle size, preferred facet and structure, the electrochemical measurements by cyclic voltammetry allows us to assess the surface area of the nanoparticles active sites. To this end, electrochemistry was used to determine the electroactive surface area (EASA) of the carbon supported Au catalyst. First, CVs were recorded in the supporting electrolyte (0.1 M KOH) in a potential window from 0.00 to 1.6V V vs. RHE. The OH desorption from Au sites occurs during the positive-going potential scan between 1.2 and 1.6 V *vs.* RHE followed by the Au surface oxidation at higher potentials.[25]

In the reverse potential scan, the Au oxide reduction corresponding to the cathodic peak takes place at 1.0 V vs. RHE. Competition between OH^-/O^{2-} anions adsorption and desorption has been well documented in the literature and is close to this potential value. [30] The Au/C catalysts electroactive surface area were determined from CV in alkaline solution. The oxide anodic stripping current peak charge integration was done by using a value of 400 μC cm^{-2} for the reduction of the oxide monolayer.[31] The EASA values obtained at a scan rate of 20 mV s^{-1} are plotted in **Figure 10**. These values are 1.88, 5.83, 13.96 and 15.0 m^2 g^{-1} for Au/C-H_2SO_4, Au/C-KBr, Au/C-KOH and Au/C-Spheres, respectively. The remarkable difference in the catalysts activity can be attributed to the pretreated carbon substrates. The distribution of Au on the carbon support surface depends on the electrolyte used for the RoDSE electrodeposition. The chloroauric acid precursor is mostly located at the particle external surface when using water, but it readily penetrates into the interior of the carbon pores in alkaline media.[32] Note that the rpm chosen in these experiments was 2000 rpm since at this rotation rate the material exhibited a higher surface area in alkaline media as shown in **Figure S4-S6**.

In **Figure 11**, shows the behavior of the electrodeposited Au NPs in KOH 0.1M (Red) and 1M Ethanol in 0.1M KOH (Black). It can be observed that in acidic and neutral media, the voltammetry profile is quite similar. Interestingly, the electrodeposition carried in alkaline media showed the most notable features of the formation of Au-OH at 1.2 V_{RHE} and the subsequent broader reduction oxide peak circa 1.1 V_{RHE} on the reverse scan. It is interesting to point out that the amount of gold determined by TGA and the current-potential profile was normalized by Au mass. Therefore, changes in activity can be attributed to changes in surface sites, responsible for the improvement in catalytic efficiency between electrolytes. The ethanol oxidation voltammetry shown in black, at a scan rate of 20 mV/s, in 1M EtOH in 0.1M KOH shows much higher

faradaic efficiencies for the Au/C-KOH primarily because of their higher surface area and the higher reactivity due to its more active surface sites.

Quasi-spherical nanoparticles were synthesized by a wet chemistry method and its activity was evaluated for ethanol electro-oxidation. The same quantity by mass of gold as Au/C KOH was deposited using the chemical reduction route. They revealed different catalytic activity towards ethanol oxidation. The voltammetry profile was similar to the Au/C-KOH however higher oxidation currents densities were obtained for the electrodeposited catalyst. The onset potential (E_{OP}) was calculated based on the CV curves from Figure 11. E_{OP} was defined as the potential where 10% of the maximum current density for the oxidation peak is generated. Values of 0.88 V, 0.85 V, 0.88 V and 0.78 V vs RHE were obtained for Au-KOH, Au-KBr and Au-H_2SO_4, and Au-Spheres respectively. In terms of onset potential, the Au-Spheres was superior to the electrodeposited catalysts. Future work involves this electrochemical methods to influence the particle shape.

Overall, the results presented for ethanol electrooxidation on gold nanoparticles closely resemble the work carried out by Tremisliosi-Filho et. al on-gold surface in alkaline media.[33, 34] The voltammetry profile results from a relatively strong interaction of the reactive species with the nanoparticles at the electrode surface. This behavior was expected according to the literature concerning the oxidation of the primary alcohols in alkaline media. There are two phenomena associated to the voltammetry observed: the deactivation of the electrode due to the formation of a passive layer and to the decrease of the ethanol concentration.

Although Au has not been considered as a standalone catalyst for EtOH electrooxidation, it has been incorporated onto many systems due to its inherent characteristic were practically no poisoning species (CO-like species) can be formed and adsorbed at the surface.[35] For example,

Zhu et al used carbon-supported gold nanoparticles (Au/C) as template for support mono-sub-monolayer palladium atoms with different Pd/Au atomic ratios resulting in a significant improvement to that the ethanol oxidation as well as a decrease in its overpotential. [36]This work could pave the future towards utilizing electrochemical methods for depositing Au nanoparticles onto carbon supports and further modifying the catalyst to enhance the reaction kinetics of ethanol electrooxidation.

A Linear Sweep Voltammetry (LSV) shown in **Figure S7** was run under the same conditions but at a 1 mV/s scan rate to examine the reaction with negligible contribution for non-faradaic current and the same trend was observed. **Figure S8** shows the stability of the catalyst at 0.700V vs. RHE and the most stable catalyst was found to be Au-NPs/C-KOH. This in part reveals the crucial role that the carbon support plays in the performance of gold nanoparticles catalyzing the oxidation of alcohols. Raman spectroscopy confirmed a restructuring of the surface sites in alkaline media, which may be responsible for the increase electrochemical performance for ethanol oxidation. The above results strongly suggest the observed catalytic activity is related to the presence of oxygen functional groups on the surface of carbon. To validate the role of O_2 functionalities on the electrocatalytic performance of the catalyst, the $I_{(C=O)}/I_{(C-O)}$ binding energy peak intensity ratio, from the XPS analyses data, was determined. Results, also suggest oxygen groups, particularly ketonic groups (R-C=O) are more likely to cause significant enhancement in the electrocatalytic activity by virtue of the strongly electron withdrawing nature of C=O functionalities which in turn cause changes in the electronic structure of its neighboring C atoms.[37]

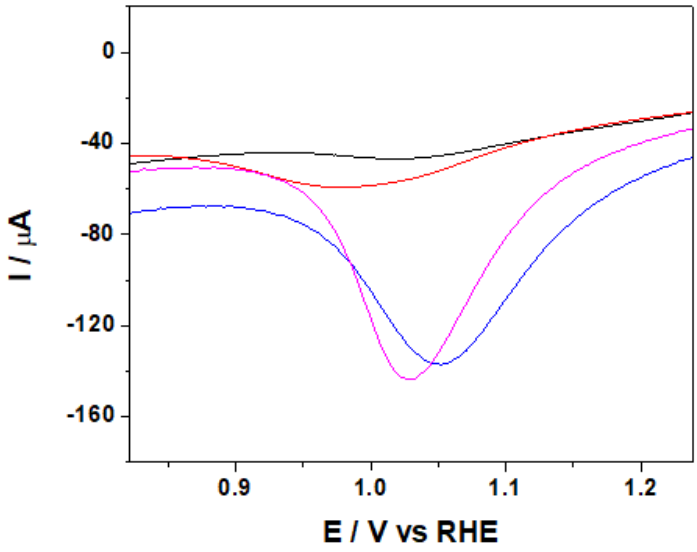

Figure 10. Linear potential sweep for the reduction of the Au-OH monolayer formed after formation of oxides at 1.6 V vs. RHE for catalysts AuNPs/C-KOH (Blue), Au/C-KBr (Red), Au/C-H_2SO_4 (Black), and Au/C-Spheres (Magenta). Scan rate was 20 mV/s.

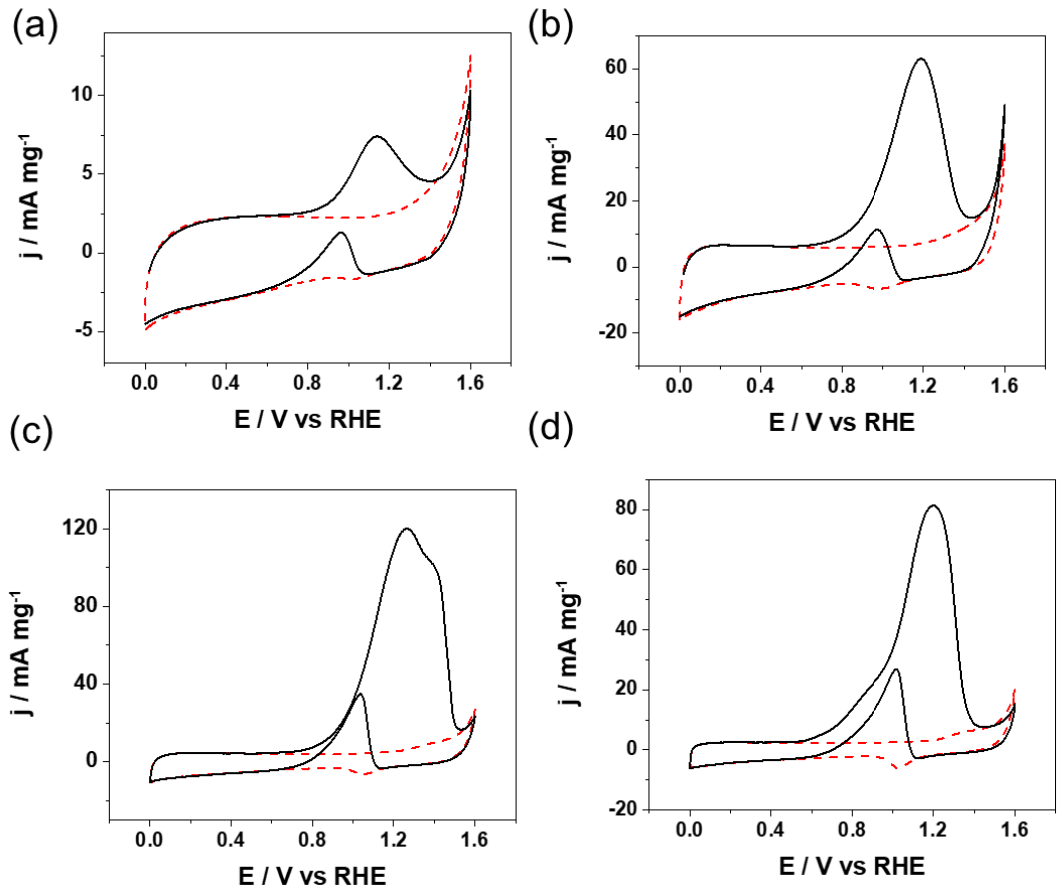

Figure 11. Cyclic Voltammetry of (a) Au/C-H_2SO_4, (b) Au/C-KBr, (c) Au/C-KOH, and (d) Au/C-Spheres analyzed via 0.1M KOH (red) and 1M EtOH in 0.1M KOH (black). Scan rate was 20 mV/s for all electrochemical measurements. The solution was Ar purged prior to any electrochemical testing.

Conclusion

In this work, we have employed an electrochemical technique to electrodeposit highly active Au nanoparticles on Vulcan XC-72R. Our results indicate a correlation between the electrolyte media composition to carbon substrate functionalities. Thus, the different substrate carbonaceous moieties act as anchoring sites for the electrodeposition of Au NPs. Moreover, electrolyte media also influenced the crystallographic structure and orientation as confirmed by XRD measurements. These changes in the surface sites and bulk structure of the Au NPs are responsible for the enhanced EtOH oxidation performance and more tolerance to poisoning than

the electrodeposited AuNP on H_2SO_4 and KBr. Our present work could be further extended to the large-scale production of highly active Au nanoparticles for fuel cell applications. It is clear that the role of the carbon support on the catalyst played an important role by (1) preventing nanoparticle agglomeration and (2) providing an adequate framework for enhanced EOR electrocatalysis.

Acknowledgements

This work was financially supported by the NSF-CREST Center for Innovation, Research and Education in Environmental Nanotechnology Grant Number HRD-1736093, NSF-PREM Center for Interfacial Electrochemistry of Energy Materials Grant Number DMR-1827622 and NASA-EPSCoR Grant Number NNX14AN18A. This research used resources of the Center for Functional Nanomaterials (CFN), which is a U.S. DOE Office of Science Facility, at Brookhaven National Laboratory (BNL) under Contract No. DE-SC0012704. LBD thanks Kim Kisslinger (CFN-BNL) for assistance on the TEM images.

References

1. Guin, S. K.; Pillai, J. S.; Ambolikar, A. S.; Saha, A.; Aggarwal, S. K., Template-free electrosynthesis of gold nanoparticles of controlled size dispersion for the determination of lead at ultratrace levels. *RSC Advances* **2013,** *3* (39), 17977-17988.
2. Antolini, E., Carbon supports for low-temperature fuel cell catalysts. *Applied Catalysis B: Environmental* **2009,** *88* (1–2), 1-24.
3. Antolini, E., Formation of carbon-supported PtM alloys for low temperature fuel cells: a review. *Materials Chemistry and Physics* **2003,** *78* (3), 563-573.
4. Solla-Gullon, J.; Vidal-Iglesias, F. J.; Feliu, J. M., Shape dependent electrocatalysis. *Annual Reports Section "C" (Physical Chemistry)* **2011,** *107* (0), 263-297.
5. Banham, D.; Ye, S., Current Status and Future Development of Catalyst Materials and Catalyst Layers for Proton Exchange Membrane Fuel Cells: An Industrial Perspective. *ACS Energy Letters* **2017,** *2* (3), 629-638.
6. Haruta, M., Catalysis: Gold rush. *Nature* **2005,** *437* (7062), 1098-1099.
7. Haruta, M., Size- and support-dependency in the catalysis of gold. *Catalysis Today* **1997,** *36* (1), 153-166.

8. Holade, Y.; Morais, C.; Servat, K.; Napporn, T. W.; Kokoh, K. B., Enhancing the available specific surface area of carbon supports to boost the electroactivity of nanostructured Pt catalysts. *Physical Chemistry Chemical Physics* **2014,** *16* (46), 25609-25620.
9. Sharma, S.; Pollet, B. G., Support materials for PEMFC and DMFC electrocatalysts—A review. *Journal of Power Sources* **2012,** *208*, 96-119.
10. Li, Z.-F.; Wang, Y.; Botte, G. G., Revisiting the electrochemical oxidation of ammonia on carbon-supported metal nanoparticle catalysts. *Electrochimica Acta* **2017,** *228* (Supplement C), 351-360.
11. Santiago, D.; Rodriguez-Calero, G. G.; Rivera, H.; Tryk, D. A.; Scibioh, M. A.; Cabrera, C. R., Platinum Electrodeposition at High Surface Area Carbon Vulcan-XC-72R Material Using a Rotating Disk-Slurry Electrode Technique. *Journal of the Electrochemical Society* **2010,** *157* (12), F189-F195.
12. Santiago, D.; Rodriguez-Calero, G. G.; Palkar, A.; Barraza-Jimenez, D.; Galvan, D. H.; Casillas, G.; Mayoral, A.; Jose-Yacaman, M.; Echegoyen, L.; Cabrera, C. R., Platinum Electrodeposition on Unsupported Carbon Nano-Onions. *Langmuir* **2012,** *28* (49), 17202-17210.
13. Contes-de Jesus, E.; Santiago, D.; Casillas, G.; Mayoral, A.; Magen, C.; Jose-Yacaman, M.; Li, J.; Cabrera, C. R., Platinum Electrodeposition on Unsupported Single Wall Carbon Nanotubes and Its Application as Methane Sensing Material. *Journal of the Electrochemical Society* **2013,** *160* (2), H98-H104.
14. Cunci, L.; Velez, C. A.; Perez, I.; Suleiman, A.; Larios, E.; José-Yacamán, M.; Watkins, J. J.; Cabrera, C. R., Platinum Electrodeposition at Unsupported Electrochemically Reduced Nanographene Oxide for Enhanced Ammonia Oxidation. *ACS Applied Materials & Interfaces* **2014,** *6* (3), 2137-2145.
15. Wei, Z. D.; Chan, S. H.; Li, L. L.; Cai, H. F.; Xia, Z. T.; Sun, C. X., Electrodepositing Pt on a Nafion-bonded carbon electrode as a catalyzed electrode for oxygen reduction reaction. *Electrochimica Acta* **2005,** *50* (11), 2279-2287.
16. Usher, A.; McPhail, D. C.; Brugger, J., A spectrophotometric study of aqueous Au(III) halide-hydroxide complexes at 25-80 degrees C. *Geochimica Et Cosmochimica Acta* **2009,** *73* (11), 3359-3380.
17. Usher, A. J.; McPhail, D. C.; Brugger, J., Spectrophotometry of Au(III)-halide complexes. *Geochimica Et Cosmochimica Acta* **2006,** *70* (18), A680-A680.
18. Santiago, D.; Cruz-Quiñonez, M.; Tryk, D. A.; Cabrera, C. R., Pt/C Catalyst Preparation Using Rotating Disk-Slurry Electrode (RoDSE) Technique. *ECS Transactions* **2007,** *3* (21), 35-40.
19. Sánchez-Sánchez, C. M.; Vidal-Iglesias, F. J.; Solla-Gullón, J.; Montiel, V.; Aldaz, A.; Feliu, J. M.; Herrero, E., Scanning electrochemical microscopy for studying electrocatalysis on shape-controlled gold nanoparticles and nanorods. *Electrochimica Acta* **2010,** *55* (27), 8252-8257.
20. Blyth, R. I. R.; Buqa, H.; Netzer, F. P.; Ramsey, M. G.; Besenhard, J. O.; Golob, P.; Winter, M., XPS studies of graphite electrode materials for lithium ion batteries. *Applied Surface Science* **2000,** *167* (1–2), 99-106.
21. Juodkazis, K.; Juodkazyt≒, J.; Jasulaitien≒, V.; Lukinskas, A.; Šebeka, B., XPS studies on the gold oxide surface layer formation. *Electrochemistry Communications* **2000,** *2* (7), 503-507.
22. Kitagawa, H.; Kojima, N.; Nakajima, T., Studies of mixed-valence states in three-dimensional halogen-bridged gold compounds, Cs2AuAuX6, (X = Cl, Br or I). Part 2. X-Ray

photoelectron spectroscopic study. *Journal of the Chemical Society, Dalton Transactions* **1991,** (11), 3121-3125.
23. Mironov, I. V., Properties of Gold(III) Hydroxide and Aquahydroxogold(III) Complexes in Aqueous Solution. *Russian Journal of Inorganic Chemistry* **2005,** *50* (7), 1115-1120.
24. MIronov, I. V.; Tsvelodub, L. D., Gold(III) Chlorohydroxo Complexes in Alkaline Aqueous Solutions. *Russian J. of Inorganic Chemistry* **2000,** *45* (4), 633-637.
25. Cherevko, S.; Zeradjanin, A. R.; Keeley, G. P.; Mayrhofer, K. J. J., A Comparative Study on Gold and Platinum Dissolution in Acidic and Alkaline Media. *Journal of The Electrochemical Society* **2014,** *161* (12), H822-H830.
26. Pesic, B.; Sergent, R. H., Reaction mechanism of gold dissolution with bromine. *Metallurgical and Materials Transactions B* **1993,** *24* (3), 419-431.
27. Guo, L.; Searson, P. C., On the influence of the nucleation overpotential on island growth in electrodeposition. *Electrochimica Acta* **2010,** *55* (13), 4086-4091.
28. Adžić, R. R.; Avramov-Ivić, M., Structural effects in electrocatalysis: Oxidation of ethylene glycol on single crystal gold electrodes in alkaline solutions. *Journal of Catalysis* **1986,** *101* (2), 532-535.
29. Kim, F.; Connor, S.; Song, H.; Kuykendall, T.; Yang, P., Platonic Gold Nanocrystals. *Angewandte Chemie International Edition* **2004,** *43* (28), 3673-3677.
30. Angerstein-Kozlowska, H.; Conway, B. E.; Hamelin, A.; Stoicoviciu, L., Elementary steps of electrochemical oxidation of single-crystal planes of Au Part II. A chemical and structural basis of oxidation of the (111) plane. *Journal of Electroanalytical Chemistry and Interfacial Electrochemistry* **1987,** *228* (1), 429-453.
31. Yeager, E.; Bockris, J. M.; Conway, B. E.; Saranapani, S., *Comprehensive treatise of electrochemistry: vol. 9, electrodiscs: experimental techniques*. Plenum Press,New York, NY: United States, 1984.
32. Lam, E.; Luong, J. H. T., Carbon Materials as Catalyst Supports and Catalysts in the Transformation of Biomass to Fuels and Chemicals. *ACS Catalysis* **2014,** *4* (10), 3393-3410.
33. Tremiliosi-Filho, G.; Gonzalez, E. R.; Motheo, A. J.; Belgsir, E. M.; Léger, J. M.; Lamy, C., Electro-oxidation of ethanol on gold: analysis of the reaction products and mechanism. *Journal of Electroanalytical Chemistry* **1998,** *444* (1), 31-39.
34. Angelucci, C. A.; Varela, H.; Tremiliosi-Filho, G.; Gomes, J. F., The significance of non-covalent interactions on the electro-oxidation of alcohols on Pt and Au in alkaline media. *Electrochemistry Communications* **2013,** *33* (0), 10-13.
35. Yan, S.; Zhang, S.; Lin, Y.; Liu, G., Electrocatalytic Performance of Gold Nanoparticles Supported on Activated Carbon for Methanol Oxidation in Alkaline Solution. *The Journal of Physical Chemistry C* **2011,** *115* (14), 6986-6993.
36. Zhu, L. D.; Zhao, T. S.; Xu, J. B.; Liang, Z. X., Preparation and characterization of carbon-supported sub-monolayer palladium decorated gold nanoparticles for the electro-oxidation of ethanol in alkaline media. *Journal of Power Sources* **2009,** *187* (1), 80-84.
37. Suryanto, B. H. R.; Zhao, C., Effect of oxygen functionalisation on the electrochemical behaviour of multiwall carbon nanotubes for alcohol oxidation reactions. *RSC Advances* **2016,** *6* (82), 78403-78408.

ASSOCIATED CONTENT Supporting Information Available: Au (III) reduction in KBr and H_2SO_4 electrolytes, additional TEM images, Raman spectra for all catalysts, RDE rpm optimization, Linear Sweep Voltammetry and Chronoamperometry of electrocatalysts for ethanol oxidation.